Research Paper
Computational Methods for Differential Equations
http://cmde.tabrizu.ac.ir
Vol. *, No. *, *, pp. 1-17
DOI:10.22034/cmde.2026.58857.2494

Numerical simulation and stability study of skin drug delivery via polymeric microneedles

Ebrahim Azhdari* **and Aram Emami**

Department of Mathematics and Computer Science, Faculty of Basic Sciences, Salman Farsi University of Kazerun, Kazerun, Iran.

Abstract

Drug delivery through reservoir-based microneedle has become highly important owing to its non-invasiveness and the ability to deliver a wide range of drugs. In this paper, we consider a system of partial differential equations to describe the transport of bounded drug, free drug and water in the reservoir, microneedle, skin and blood vessel. The system of equations is completed with interface boundary conditions, initial and boundary conditions. Additionally, the initial and boundary value problem is studied from an analytical point of view for stability, and from a numerical point of view for qualitative behaviour. Finally, it is shown that the results agree well with the experimental data.

Keywords. Mathematical modelling, Drug delivery, Viscoelastic, Numerical simulations, Stability analysis.

2010 Mathematics Subject Classification. 65M06, 65M12.

1. Introduction

The skin is one of the ways through which drug could be delivered with local and systemic effectiveness. The stratum corneum is the outermost layer of the skin and the main defense barrier for the drug to pass through, which leads to a decrease in the effectiveness of the drug [21]. On the other hand, subcutaneous injection is painful and usually rejected by patients. In order to overcome these problems, new drug delivery technologies have been emerged [12].

Over the last two decades, the drug delivery system using microneedles has been considered as a conventional method for delivering vaccines, drugs and cosmetics [14]. A microneedle consists of micron-sized needles allowing drug molecules to pass through the last layer of the skin and painlessly enter the inner layers of it [9, 13, 19].

In general, microneedles are divided into five categories, namely solid, hollow, coated, dissolving, and swellable microneedles [5, 8, 22, 25, 30]. Solid microneedle enhances drug absorption through the skin by creating microscopic openings, but does not contain active ingredients. After removal of the solid microneedle, semi-solid products, like creams or patches, should be used. On the other hand, hollow microneedle delivers liquid products through its hollow needle holes, acting as a medicinal reservoir for slow skin penetration. Coated microneedles however are solid needles with a medicine coating, with the microneedle penetrating the skin and releasing the drug into lower layers. Of note, the ingredients of the dissolved microneedles are water-soluble or biodegradable materials, such as sugar and polymer, and the drug is encapsulated inside the matrix. After being used on the surface of the skin, they are completely dissolved or destroyed. Through these microneedles, the drug is injected under the stratum corneum, without any dangerous residue on the surface of the skin after use. Furthermore, swellable microneedles release drugs into the skin by swelling and absorbing body fluids.

The materials used in the preparation and manufacturing of microneedles should comprise neutral materials, not causing sensitivity, high mechanical strength or high biocompatibility. The materials used to make microneedles include silicon, metal, glass, ceramide, polymers and sugar [12]. Herein, the microneedles used were made of polymers.

Received: 16 October 2023; Accepted: 04 July 2026.
∗ Corresponding author. Email: e.azhdari@kazerunsfu.ac.ir.

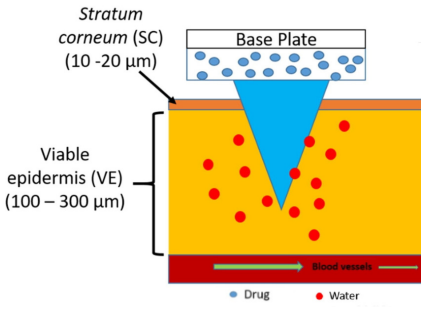

FIGURE 1. Mechanism of microneedles drug delivery.

There has been a great body of evidence concerning the use of different types of polymers as microneedles. Clearly, there is dire need for organizing and optimizing the laboratory results in order to maximize the use of these microneedles [28]. In this regard, mathematical modeling saves time and reduces laboratory defects. The modeling considers different concentrations, including bounded drug, free drug and water in the reservoir, microneedle, skin and blood vessels [26]. Several studies have been conducted on the optimization of all types of microneedles in different dimensions [29–32]. In these models, some medicine is loaded in a reservoir connected to the microneedle. After contact with the water that reaches the reservoir from the skin, the drug breaks down and turns into free drug. Finally, the drug starts to spread and reaches the blood vessel through the skin [11, 20].

To describe drug delivery through microneedles, many models have been presented, each of which deals with different aspects of this category [1, 5, 6, 10, 13]. None of them has however considered the mechanical property caused by the viscoelasticity of the polymer, in which changes Fick's second law, interpreted as non-Fickian law [2, 16]. In this paper, we used Maxwell model to consider the relationship between stress and strain [7]. This mechanical property of the polymeric microneedle acts as a barrier against the infiltration of water from the skin into the microneedle and delays the infiltration of water into the reservoir, thus affecting the drug's decomposition. Therefore, the study of this model is highly conducive to increasing the accuracy of drug delivery through microneedles. Additionally, herein, to study the stability of the problem, due to the non-linearity of the equations in the reactive sentences, we acted through linearization around short and long times. To study the effect of the parameters and analyze the sensitivity of the data, we solved the problem numerically and checked the error caused by using the numerical method. Note that the model developed in this paper agrees with the experimental and simulation results in Paper [31]. As can be seen from the results, about 20% of the initial loaded drug has been distributed in 24 hours.

This paper is summarized in several sections as follows: In section 2, we present the model and the initial and boundary conditions. Section 3 however presents the stability study of the model by linearizing the equations around short and long times while in section 4, we report numerical results and data sensitivity analysis study. Finally, in section 5, we discuss the conclusions and future work.

2. MATHEMATICAL MODEL

Assuming that the microneedle enters the skin with a polymeric property and causes slight changes in the skin that we ignore . It is assumed that the polymeric microneedle has viscoelastic properties [27, 29]. The reservoir that is actually attached to the microneedle base contains the drug (Figure 1. About 60 to 75% of the skin is made up of water [18]. After the microneedle penetrates the skin, the water inside the skin is collected around the microneedle, and due to the absorbent property of the microneedle, the water penetrates into the microneedle. From there, the water enters the drug reservoir and reacts with the drug molecules. It causes the drug to be released. Due to the difference in concentration, the released drugs enter the microneedle and from there, enter the skin and finally into the circulatory system.

2.1. **Governing equation.** In this study, a two-dimensional model of the insertion of a microneedle (Ω_m) into the skin (Ω_s) with a reservoir (Ω_r) attached to the back containing the drug is developed (Figure 2). At the end of the

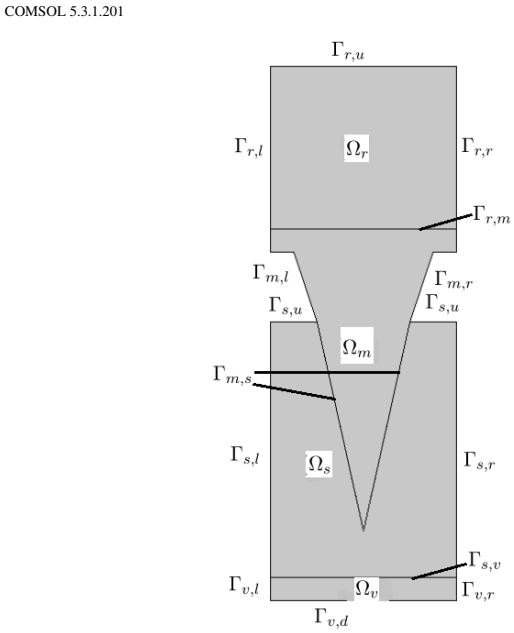

FIGURE 2. Computational domain and nomenclature of boundaries and interface boundaries.

skin, there is a blood vessel (Ω_v). The boundaries of the reservoir are indicated by $\Gamma_{r,l}$, $\Gamma_{r,r}$ and $\Gamma_{r,u}$. The interface boundary of the reservoir and the microneedle is marked with $\Gamma_{r,m}$. The outer boudary of the microneedle, which is outside the skin, is indicated by $\Gamma_{m,l}$ and $\Gamma_{m,r}$. $\Gamma_{m,s}$ is the interface boundary between microneedle and skin. Skin boundaries are indicated by $\Gamma_{s,l}$, $\Gamma_{s,r}$ and $\Gamma_{s,u}$. The interface boundary of skin and blood vessel is indicated by $\Gamma_{s,v}$. Finally, the blood vessel boundaries are $\Gamma_{v,l}$, $\Gamma_{v,r}$ and $\Gamma_{v,d}$.

As described above, diffusion-reaction equations are used to transport water and drug from reservoir, microneedle, and skin. The device consists of three components: water, bounded drug and free drug. At first, there is only the bounded drug in the reservoir, which turns into a free drug after entering the water. Since the microneedle tends to absorb free drugs due to its polymer property, so some of the free drug entered into the microneedle is absorbed by the microneedle and becomes a bounded drug [24]. Similarly, some of the free drug that entered into the skin reacts with cell receptors and becomes bounded drug [23].

As the reservoir absorbs water from the skin through the microneedle, the drug in the reservoir dissolves in response to incoming water and becomes a free drug and is ready to be dispensed. Therefore, to describe this phenomenon in the reservoir, we use the following equations:

$$\frac{\partial C_{f,r}}{\partial t} = \nabla.(D_{f,r}\nabla C_{f,r}) + k_r C_{b,r} C_{w,r}, \tag{2.1}$$

$$\frac{\partial C_{b,r}}{\partial t} = -k_r C_{b,r} C_{w,r}, \tag{2.2}$$

$$\frac{\partial C_{w,r}}{\partial t} = \nabla.(D_{w,r}\nabla C_{w,r}) - k_r C_{b,r} C_{w,r}, \tag{2.3}$$

where $C_{i,r}, i = f, b, w$ represent free drug, bounded drug and water concentration, respectively, $D_{i,r}, i = f, w$ are free drug diffusion coefficient and water diffusion coefficient in the reservoir, respectively and k_r is the solubilisation rate constant.

The free drug released from the reservoir enters the microneedle. The polymeric microneedle retains some of the released drug due to the drug's contact with the polymer. The viscoelastic property of microneedles, which prevents water from entering the skin, is considered here, which has not been considered in the previous papers. The drug

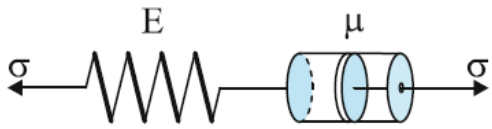

FIGURE 3. Maxwell fluid model.

enters the skin after microneedle. Similarly, some of the drug is metabolized in the skin by skin cells. Therefore, the equations that measure the amount of drug and water inside the microneedle and the skin are as follows:

$$\frac{\partial C_{f,i}}{\partial t} = \nabla.(D_{f,i}\nabla C_{f,i}) - k_i C_{f,i}, \tag{2.4}$$

$$\frac{\partial C_{b,i}}{\partial t} = k_i C_{f,i}, \tag{2.5}$$

$$\frac{\partial C_{w,i}}{\partial t} = \nabla.(D_{w,i}\nabla C_{w,i}), \tag{2.6}$$

for $i = m, s$, where $C_{f,i}, C_{b,i}, C_{w,i}, i = m, s$ are free drug, bounded drug and water concentration in microneedle when $i = m$ and skin when $i = s$ and $k_i, i = m, s$ are the binding rate constants in microneedle and skin, respectively.

To consider the viscoelastic properties of the polymeric microneedle, $\nabla.(D_\sigma\nabla\sigma)$ is added to (2.6) and for the microneedle, (2.6) will be as follows:

$$\frac{\partial C_{w,m}}{\partial t} = \nabla.(D_{w,m}\nabla C_{w,m}) + \nabla.(D_\sigma\nabla\sigma), \tag{2.7}$$

where σ is the stress and D_σ is the viscoelastic diffusion coefficient. In fact, this sentence is a description of the mechanical properties of polymeric materials. In other words, this statement states that the microneedle acts as a barrier against the penetration of water through the skin.

In order to consider the mechanical properties of polymeric microneedle, we bring the Maxwell model to define the relationship between stress and strain. In this model, a damper and a spring are connected in series (Figure 3). The model obtained after mathematical operations on it, is as follows [7]:

$$\frac{\partial \sigma}{\partial t} + \frac{E}{\mu}\sigma = E\frac{\partial \epsilon}{\partial t}, \tag{2.8}$$

where ϵ is the strain, E denotes the Young modulus of the spring and μ denotes the viscosity of the damper.

In the last equation, according to [17], we assume that strain is a linear function of water, in other words $\epsilon = f(C_{w,m})$. Also, to show that the polymeric microneedle acts as a barrier against water entering from the skin, like [2–4], we consider a minus sign on the right side of the last equation. Therefore, after these explanations, the last equation becomes as follows:

$$\frac{\partial \sigma}{\partial t} + \frac{E}{\mu}\sigma = -E\frac{\partial C_{w,m}}{\partial t}. \tag{2.9}$$

After passing through the skin, the drug enters the circulatory system in the blood vessels. The advection-diffusion equation is used to describe the drug concentration, $C_{f,v}$, in the blood vessel. Therefore, this equation is as follows:

$$\frac{\partial C_{f,v}}{\partial t} + \mathbf{v}.\nabla C_{f,v} = \nabla.(D_{f,v}\nabla C_{f,v}), \tag{2.10}$$

where $D_{f,v}$ is the diffusion coefficient of free drug in blood vessel and $\mathbf{v}$ is the velocity of drug in blood flow and is described by the incompressible Navier-Stokes equation as follows [4]:

$$\begin{cases} \rho\dfrac{\partial \mathbf{v}}{\partial t} - \nabla.\mu_b(\nabla\mathbf{v} + (\nabla\mathbf{v})^T) + \rho(\mathbf{v}.\nabla)\mathbf{v} + \nabla p = 0, \\ \rho.\nabla\mathbf{v} = 0, \end{cases} \tag{2.11}$$

where ρ is the blood density, μ_b is the blood viscosity and p is the pressure.

2.2. **Initial, boundary and interface conditions.** Inside the reservoir:

$$C_{f,r} = 0, C_{b,r} = c_{b,r_0}, C_{w,r} = 0, \ at\ t = 0, \tag{2.12}$$

where c_{b,r_0} is the initial bounded drug which is loaded in the reservoir.
Inside the microneedle:

$$C_{f,m} = 0, C_{b,m} = 0, C_{w,m} = 0, \ at\ t = 0, \tag{2.13}$$

Inside the skin:

$$C_{f,s} = 0, C_{b,s} = 0, C_{w,s} = c_{w,s_0}, \ at\ t = 0, \tag{2.14}$$

where c_{w,s_0} is the initial water in the skin.
Inside the blood vessels:

$$C_{f,v} = 0, \mathbf{v} = 0, p = 0, \ at\ t = 0. \tag{2.15}$$

In parts of the reservoir, microneedle located outside the skin and skin, no flux boundary condition is assumed as following:

$$D_{f,r}\nabla C_{f,r} \cdot \eta_r = 0, D_{w,r}\nabla C_{w,r} \cdot \eta_r = 0, \tag{2.16}$$

$$D_{f,m}\nabla C_{f,m} \cdot \eta_m = 0, D_{w,m}\nabla C_{w,m} \cdot \eta_m = 0, \tag{2.17}$$

$$D_{f,s}\nabla C_{f,s} \cdot \eta_s = 0, (D_{w,s}\nabla C_{w,s} + D_\sigma \nabla\sigma) \cdot \eta_s = 0, \tag{2.18}$$

where $\eta_i, i = r, m, s$ are the exterior unit normal.
In blood vessel the following boundary conditions are assumed for the free drug concentration and velocity:

$$(D_{f,v}\nabla C_{f,v} - \mathbf{v}C_{f,v}) \cdot \eta_v = 0, \tag{2.19}$$

$$C_{f,v} = 0, \tag{2.20}$$

$$\mathbf{v} = U, \tag{2.21}$$

$$\mathbf{v} = 0, \tag{2.22}$$

$$p = 0, \tag{2.23}$$

where η_v is the exterior unit normal and U is the maximum flow velocity at the inlet of the blood vessel.

The boundary conditions considered in the model, are shown in the Figure 4.

The interface boundary conditions for the free drug concentration and water are considered as following, respectively:

$$\begin{cases} D_{f,r}\nabla C_{f,r} \cdot \eta_r = \iota_{r,m}(C_{f,r} - C_{f,m}), \\ D_{f,m}\nabla C_{f,m} \cdot \eta_m = -D_{f,r}\nabla C_{f,r} \cdot \eta_r, \\ D_{f,m}\nabla C_{f,m} \cdot \eta_m = \iota_{m,s}(C_{f,m} - C_{f,s}), \\ D_{f,s}\nabla C_{f,s} \cdot \eta_s = -D_{f,m}\nabla C_{f,m} \cdot \eta_m, \\ D_{f,s}\nabla C_{f,s} \cdot \eta_s = \iota_{s,v}(C_{f,s} - C_{f,v}), \\ (D_{f,v}\nabla C_{f,v} - \mathbf{v}C_{f,v}) \cdot \eta_v = -D_{f,s}\nabla C_{f,s} \cdot \eta_s, \end{cases} \tag{2.24}$$

and

$$\begin{cases} D_{w,s}\nabla C_{w,s} \cdot \eta_s = \iota_{m,s}(C_{w,s} - C_{w,m}), \\ (D_{w,m}\nabla C_{w,m} + D_\sigma\nabla\sigma) \cdot \eta_m = -D_{w,s}\nabla C_{w,s} \cdot \eta_s, \\ (D_{w,m}\nabla C_{w,m} + D_\sigma\nabla\sigma) \cdot \eta_m = \iota_{r,m}(C_{w,m} - C_{w,r}), \\ D_{w,r}\nabla C_{w,r} \cdot \eta_r = -(D_{w,m}\nabla C_{w,m} + D_\sigma\nabla\sigma) \cdot \eta_m, \end{cases} \tag{2.25}$$

where $\iota_{r,m}, \iota_{m,s}, \iota_{s,v}$ are the partition coefficients of the interfaces.

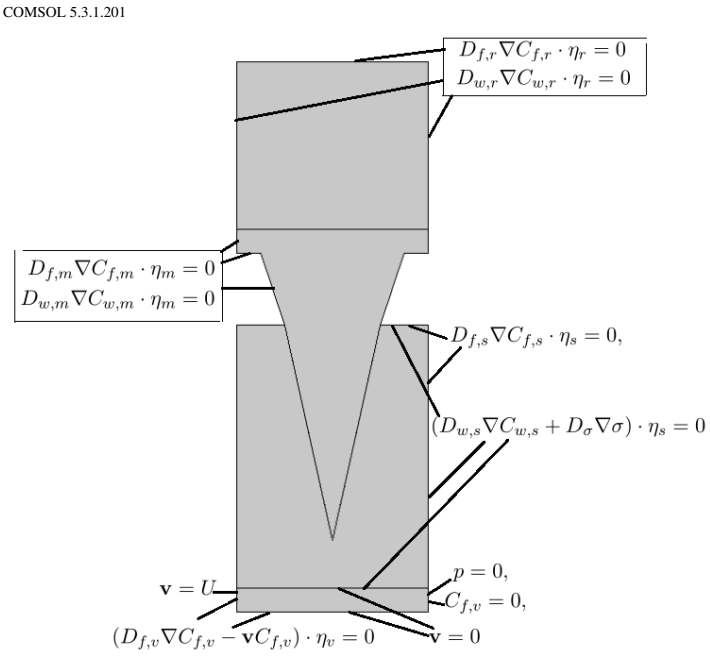

FIGURE 4. Boundary conditions for different domains.

3. THEORETICAL RESULTS

To study the stability behaviour of problem (2.1)-(2.25), we need to linearize problem (2.1)-(2.3) for short and long times. For short times, the system is linearized in the neighborhood of the initial state, and for long times, the system is linearized in the neighborhood of the static solution. Let $\tilde{C}_{f,r}$, $\tilde{C}_{b,r}$ and $\tilde{C}_{w,r}$ be a solution of (2.1)-(2.3). The linearized system at this solution can be written in the following form

$$\frac{\partial C_{f,r}}{\partial t}=\nabla.(D_{f,r}\nabla C_{f,r})+k_r\tilde{C}_{b,r}C_{w,r}+k_rC_{b,r}\tilde{C}_{w,r}, \tag{3.1}$$

$$\frac{\partial C_{b,r}}{\partial t}=-k_r\tilde{C}_{b,r}C_{w,r}-k_rC_{b,r}\tilde{C}_{w,r}, \tag{3.2}$$

$$\frac{\partial C_{w,r}}{\partial t}=\nabla.(D_{w,r}\nabla C_{w,r})-k_r\tilde{C}_{b,r}C_{w,r}-k_rC_{b,r}\tilde{C}_{w,r}. \tag{3.3}$$

For small times the concentration of water in the reservoir is very small so we consider

$$\tilde{C}_{w,r}=0,\tilde{C}_{b,r}=c_{b,r_0}.$$

For large times, that is when the bounded drug changed to free drug and released and the reservoir is full of water, we assume

$$\tilde{C}_{w,r}=c_{w,s_0},\tilde{C}_{b,r}=0.$$

Stability for short times: In this case, Equations (3.1)-(3.3) become

$$\frac{\partial C_{f,r}}{\partial t}=\nabla.(D_{f,r}\nabla C_{f,r})+k_rc_{b,r_0}C_{w,r}, \tag{3.4}$$

$$\frac{\partial C_{b,r}}{\partial t}=-k_rc_{b,r_0}C_{w,r}, \tag{3.5}$$

$$\frac{\partial C_{w,r}}{\partial t}=\nabla.(D_{w,r}\nabla C_{w,r})-k_rc_{b,r_0}C_{w,r}. \tag{3.6}$$

In what follows we use the energy method to analyze (2.4)-(2.25) and (3.4)-(3.6).

From (2.9) and by considering $C_{w,m}(0)=0$ we easily get

$$\sigma=\frac{E^2}{\mu}\int_0^t e^{-\frac{E}{\mu}(t-s)}C_{w,m}(s)ds-EC_{w,m}(t)+\sigma(0)e^{-\frac{E}{\mu}t},$$

and using this equality in the (2.7) and considering $\sigma(0)$ is constant, we obtain for $C_{w,m}$ the following equation

$$\begin{aligned}\frac{\partial C_{w,m}}{\partial t}&=\nabla.(D_{w,m}\nabla C_{w,m})+\nabla.\Big(D_\sigma\nabla(\frac{E^2}{\mu}\int_0^t e^{-\frac{E}{\mu}(t-s)}C_{w,m}(s)ds-EC_{w,m}(t)+\sigma(0)e^{-\frac{E}{\mu}t})\Big)\\&=\nabla.(D_{w,m}\nabla C_{w,m})+\int_0^t e^{-\frac{E}{\mu}(t-s)}\nabla.(\frac{E^2}{\mu}D_\sigma\nabla C_{w,m}(s))ds+\nabla.((-ED_\sigma)\nabla C_{w,m})\\&+\nabla.(e^{-\frac{E}{\mu}t}\nabla\sigma(0))=\nabla.((D_{w,m}-ED_\sigma)\nabla C_{w,m})+\int_0^t e^{-\frac{E}{\mu}(t-s)}\nabla.(\frac{E^2}{\mu}D_\sigma\nabla C_{w,m}(s))ds,\end{aligned}$$

therefore

$$\frac{\partial C_{w,m}}{\partial t}=\nabla.(D_{w,m}\nabla C_{w,m})+\int_0^t e^{-\frac{E}{\mu}(t-s)}\nabla.(D_v\nabla C_{w,m}(s))ds, \tag{3.7}$$

where $D_{w,m}=D_{w,m}-ED_\sigma$ and $D_v=\frac{E^2}{\mu}D_\sigma$.

Let $V=[H^1(\Omega_r)]^2\times L^2(\Omega_r)\times[H^1(\Omega_m)]^2\times L^2(\Omega_m)\times[H^1(\Omega_s)]^2\times L^2(\Omega_s)\times H^1(\Omega_v)$ and let $c=(C_{f,r},C_{w,r},C_{b,r},C_{f,m},C_{w,m},C_{b,m},C_{f,s},C_{w,s},C_{b,s},C_{f,v})\in V$, then we have

$$\begin{aligned}&\sum_{j=r,m,s}\sum_{i=f,b,w}(\frac{\partial C_{i,j}}{\partial t},v_{i,j})_{\Omega_j}+(\frac{\partial C_{f,v}}{\partial t},v_{f,v})_{\Omega_v}+\sum_{j=r,m,s}\sum_{i=f,w}(D_{i,j}\nabla C_{i,j},\nabla v_{i,j})_{\Omega_j}\\&+\int_0^t e^{-\frac{E}{\mu}(t-s)}(D_v\nabla C_{w,m}(s),\nabla v_{w,m})ds\\&+(D_{f,v}\nabla C_{f,v},\nabla v_{f,v})_{\Omega_v}+(\mathbf{v}.\nabla C_{f,v},v_{f,v})_{\Omega_v}\\&+k_rc_{b,r_0}(C_{w,r},v_{f,r}-v_{b,r}-v_{w,r})_{\Omega_r}\\&-\sum_{j=m,s}k_j(C_{f,j},v_{f,j}-v_{b,j})_{\Omega_j}\\&=-(\iota_{r,m}[C_f(t)],[v_f])_{\Gamma_{r,m}}-(\iota_{m,s}[C_f(t)],[v_f])_{\Gamma_{m,s}}\\&-(\iota_{s,v}[C_f(t)],[v_f])_{\Gamma_{s,v}}-(\iota_{m,s}[C_w(t)],[v_w])_{\Gamma_{m,s}}\\&-(\iota_{r,m}[C_w(t)],[v_w])_{\Gamma_{r,m}},\end{aligned} \tag{3.8}$$

for all $v_{i,j},j=r,m,s,i=f,b,w$ and $v_{f,v}$ in V and $c(0)=(0,0,c_{b,r_0},0,0,0,0,c_{w,s_0},0,0)$.
In (3.8) the following notations were used:

$$(\iota_{r,m}[C_f(t)],[v_f])_{\Gamma_{r,m}}=\int_{\Gamma_{r,m}}\iota_{r,m}[C_f(t)][v_f]d\mu,$$

$$[C_f(t)]=C_{f,r}(t)-C_{f,m}(t),[v_f(t)]=v_{f,r}-v_{f,m},$$

$C_{f,r},C_{f,m},v_{f,r},v_{f,m}$ on $\Gamma_{r,m}$ are given by Trace Theorem [15]). In (3.8) $(\iota_{m,s}[C_f(t)],[v_f])_{\Gamma_{m,s}}$, $(\iota_{s,v}[C_f(t)],[v_f])_{\Gamma_{s,v}}$, $(\iota_{m,s}[C_w(t)],[v_w])_{\Gamma_{m,s}}$ and $(\iota_{r,m}[C_w(t)],[v_w])_{\Gamma_{r,m}}$ are defined analogously.

We establish in what follows an estimate for the energy functional

$$\begin{aligned}\varepsilon(c(t))&=\sum_{j=r,m,s}\sum_{i=f,b,w}\|C_{i,j}(t)\|^2_{\Omega_j}+\|C_{f,v}(t)\|^2_{\Omega_v}+\sum_{j=r,m,s}\sum_{i=f,w}\int_0^t\|\nabla C_{i,j}(s)\|^2_{\Omega_j}ds\\&+\int_0^t\|\nabla C_{f,v}(s)\|^2_{\Omega_v}ds+\int_0^t\big(\|[C_f(s)]\|^2_{\Gamma_{r,m}\cup\Gamma_{m,s}\cup\Gamma_{s,v}}+\|[C_w(s)]\|^2_{\Gamma_{m,s}\cup\Gamma_{r,m}}\big)ds.\end{aligned} \tag{3.9}$$

Theorem 3.1. *Let $c \in V$ be a solution of the variational problem (3.8). Then*

$$\varepsilon(c(t)) \leq \varepsilon(c(0))e^{\Phi t}, \tag{3.10}$$

where $\epsilon_1, \epsilon_6 \neq 0$ satisfy

$$D_{f,v} - \epsilon_1^2 > 0, \ D_{w,m} - \epsilon_6^2 > 0, \tag{3.11}$$

and

$$\Phi = \frac{\min\{2D_{i,j}, 2(D_{f,v} - \epsilon_1^2), 2(D_{w,m} - \epsilon_6^2), \max\{2\iota_{r,m}, 2\iota_{m,s}, 2\iota_{s,v}\}\}}{\max\{\frac{D_v^2\mu}{4\epsilon_6^2 E}, \frac{1}{2\epsilon_1^2}\|\mathbf{v}\|^2_{L^\infty(\Omega_v)}, 2(k_r c_{b,r_0} + k_r^2 c_{b,r_0}^2(\epsilon_2^2 + \epsilon_3^2)), 2(k_m + k_m^2\epsilon_4^2), 2(k_s + k_s^2\epsilon_5^2), \frac{1}{2\epsilon_z^2}, \}}, \tag{3.12}$$

where $i = f, b, w, j = r, m, s, z = 2, 3, 4, 5$.

Proof. Taking in (3.8) $v_{i,j} = C_{i,j}, i = f, b, w, j = r, m, s$ and $v_{f,v} = C_{f,v}$, we easily obtain

$$\begin{aligned}
&\frac{1}{2}\sum_{j=r,m,s}\sum_{i=f,b,w}\frac{d}{dt}\|C_{i,j}(t)\|^2_{\Omega_j} + \frac{1}{2}\frac{d}{dt}\|C_{f,v}(t)\|^2_{\Omega_v} \\
&+ \sum_{j=r,m,s}\sum_{i=f,w} D_{i,j}\|\nabla C_{i,j}(t)\|^2_{\Omega_j} + \int_0^t e^{-\frac{E}{\mu}(t-s)}(D_v\nabla C_{w,m}(s), \nabla C_{w,m})ds \\
&+ D_{f,v}\|\nabla C_{f,v}(t)\|^2_{\Omega_v} + (\mathbf{v}.\nabla C_{f,v}, C_{f,v})_{\Omega_v} - k_r c_{b,r_0}\|C_{w,r}(t)\|^2_{\Omega_r} \\
&+ k_r c_{b,r_0}(C_{w,r}, C_{f,r})_{\Omega_r} - k_r c_{b,r_0}(C_{w,r}, C_{b,r})_{\Omega_r} - k_m\|C_{f,m}(t)\|^2_{\Omega_m} \\
&+ k_m(C_{f,m}, C_{b,m})_{\Omega_m} - k_s\|C_{f,s}(t)\|^2_{\Omega_s} + k_s(C_{f,s}, C_{b,s})_{\Omega_s} \\
&= -\iota_{r,m}\|[C_f(t)]\|^2_{\Gamma_{r,m}} - \iota_{m,s}\|[C_f(t)]\|^2_{\Gamma_{m,s}} - \iota_{s,v}\|[C_f(t)]\|^2_{\Gamma_{s,v}} \\
&- \iota_{m,s}\|[C_w(t)]\|^2_{\Gamma_{m,s}} - \iota_{r,m}\|[C_w(t)]\|^2_{\Gamma_{r,m}}.
\end{aligned} \tag{3.13}$$

For any non zero constants $\epsilon_i, i = 1, \cdots, 6$ we have the following inequalities

$$(\mathbf{v}.\nabla C_{f,v}, C_{f,v})_{\Omega_v} \leq \frac{1}{4\epsilon_1^2}\|\mathbf{v}(t)\|^2_{L^\infty(\Omega_v)}\|C_{f,v}(t)\|^2_{\Omega_v} + \epsilon_1^2\|\nabla C_{f,v}(t)\|^2_{\Omega_v}, \tag{3.14}$$

$$k_r c_{b,r_0}(C_{w,r}, C_{f,r})_{\Omega_r} \leq k_r^2 c_{b,r_0}^2\epsilon_2^2\|C_{w,r}(t)\|^2_{\Omega_r} + \frac{1}{4\epsilon_2^2}\|C_{f,r}(t)\|^2_{\Omega_r}, \tag{3.15}$$

$$-k_r c_{b,r_0}(C_{w,r}, C_{b,r})_{\Omega_r} \leq k_r^2 c_{b,r_0}^2\epsilon_3^2\|C_{w,r}(t)\|^2_{\Omega_r} + \frac{1}{4\epsilon_3^2}\|C_{b,r}(t)\|^2_{\Omega_r}, \tag{3.16}$$

$$k_m(C_{f,m}, C_{b,m})_{\Omega_m} \leq k_m^2\epsilon_4^2\|C_{f,m}(t)\|^2_{\Omega_m} + \frac{1}{4\epsilon_4^2}\|C_{b,m}(t)\|^2_{\Omega_m}, \tag{3.17}$$

$$k_s(C_{f,s}, C_{b,s})_{\Omega_s} \leq k_s^2\epsilon_5^2\|C_{f,s}(t)\|^2_{\Omega_s} + \frac{1}{4\epsilon_5^2}\|C_{b,s}(t)\|^2_{\Omega_s}, \tag{3.18}$$

$$\int_0^t e^{-\frac{E}{\mu}(t-s)}(D_v\nabla C_{w,m}(s), \nabla C_{w,m})ds \leq \epsilon_6^2\|\nabla C_{w,m}(t)\|^2_{\Omega_m} + \frac{D_v^2\mu}{8\epsilon_6^2 E}\int_0^t \|\nabla C_{w,m}(s)\|^2_{\Omega_m}ds. \tag{3.19}$$

Using the inequalities (3.14)-(3.19) in (3.13) we obtain

$$\sum_{j=r,m,s}\sum_{i=f,b,w}\frac{d}{dt}\|C_{i,j}(t)\|^2_{\Omega_j}+\frac{d}{dt}\|C_{f,v}(t)\|^2_{\Omega_v}+\sum_{j=r,m,s}\sum_{i=f,w}2D_{i,j}\|\nabla C_{i,j}(t)\|^2_{\Omega_j}$$
$$+2(D_{f,v}-\epsilon_1^2)\|\nabla C_{f,v}(t)\|^2_{\Omega_v}+2(D_{w,m}-\epsilon_6^2)\|\nabla C_{w,m}(t)\|^2_{\Omega_m}$$
$$+\max\{2\iota_{r,m},2\iota_{m,s},2\iota_{s,v}\}\big(\|[C_f(t)]\|^2_{\Gamma_{r,m}\cup\Gamma_{m,s}\cup\Gamma_{s,v}}+\|[C_w(t)]\|^2_{\Gamma_{m,s}\cup\Gamma_{r,m}}\big)$$
$$\leq\frac{D_v^2\mu}{4\epsilon_6^2E}\int_0^t\|\nabla C_{w,m}(s)\|^2_{\Omega_m}ds+\frac{1}{2\epsilon_1^2}\|\mathbf{v}(t)\|^2_{L^\infty(\Omega_v)}\|C_{f,v}(t)\|^2_{\Omega_v}$$
$$+2(k_rc_{b,r_0}+k_r^2c_{b,r_0}^2(\epsilon_2^2+\epsilon_3^2))\|C_{w,r}(t)\|^2_{\Omega_r}+2(k_m+k_m^2\epsilon_4^2)\|C_{f,m}(t)\|^2_{\Omega_m}$$
$$+2(k_s+k_s^2\epsilon_5^2)\|C_{f,s}(t)\|^2_{\Omega_s}+\frac{1}{2\epsilon_2^2}\|C_{f,r}(t)\|^2_{\Omega_r}+\frac{1}{2\epsilon_3^2}\|C_{b,r}(t)\|^2_{\Omega_r}$$
$$+\frac{1}{2\epsilon_4^2}\|C_{b,m}(t)\|^2_{\Omega_m}+\frac{1}{2\epsilon_5^2}\|C_{b,s}(t)\|^2_{\Omega_s}. \tag{3.20}$$

If we fix ϵ_1,ϵ_6 satisfying (3.11) then

$$\varepsilon(c(t))\leq\Phi\int_0^t\varepsilon(c(s))ds+\varepsilon(c(0)),$$

where Φ is defined by (3.12). Finally by using Gronwall's Lemma we obtain (3.10). □

From inequality (3.10), we can conclude the uniqueness of the solution of the (3.8) and also the stability of this solution in a limited time interval.

Stability for large times: In this case the equations (3.1)-(3.3) become

$$\frac{\partial C_{f,r}}{\partial t}=\nabla.(D_{f,r}\nabla C_{f,r})+k_rc_{w,s_0}C_{b,r}, \tag{3.21}$$
$$\frac{\partial C_{b,r}}{\partial t}=-k_rc_{w,s_0}C_{b,r}, \tag{3.22}$$
$$\frac{\partial C_{w,r}}{\partial t}=\nabla.(D_{w,r}\nabla C_{w,r})-k_rc_{w,s_0}C_{b,r}. \tag{3.23}$$

For this case the variational formulation (3.8) becomes

$$\sum_{j=r,m,s}\sum_{i=f,b,w}(\frac{\partial C_{i,j}}{\partial t},v_{i,j})_{\Omega_j}+(\frac{\partial C_{f,v}}{\partial t},v_{f,v})_{\Omega_v}+\sum_{j=r,m,s}\sum_{i=f,w}(D_{i,j}\nabla C_{i,j},\nabla v_{i,j})_{\Omega_j}$$
$$+\int_0^t e^{-\frac{E}{\mu}(t-s)}(D_v\nabla C_{w,m}(s),\nabla v_{w,m})ds$$
$$+(D_{f,v}\nabla C_{f,v},\nabla v_{f,v})_{\Omega_v}+(\mathbf{v}.\nabla C_{f,v},v_{f,v})_{\Omega_v}$$
$$+k_rc_{w,s_0}(C_{b,r},v_{f,r}-v_{b,r}-v_{w,r})_{\Omega_r}$$
$$-\sum_{j=m,s}k_j(C_{f,j},v_{f,j}-v_{b,j})_{\Omega_j}$$
$$=-(\iota_{r,m}[C_f(t)],[v_f])_{\Gamma_{r,m}}-(\iota_{m,s}[C_f(t)],[v_f])_{\Gamma_{m,s}}$$
$$-(\iota_{s,v}[C_f(t)],[v_f])_{\Gamma_{s,v}}-(\iota_{m,s}[C_w(t)],[v_w])_{\Gamma_{m,s}}$$
$$-(\iota_{r,m}[C_w(t)],[v_w])_{\Gamma_{r,m}}. \tag{3.24}$$

Following the proof of Theorem 3.1, we can get the Theorem 3.2 as following.

Theorem 3.2. *Let $c\in V$ be a solution of the variational problem (3.24). Then*

$$\varepsilon(c(t))\leq\varepsilon(c(0))e^{\Phi t}, \tag{3.25}$$

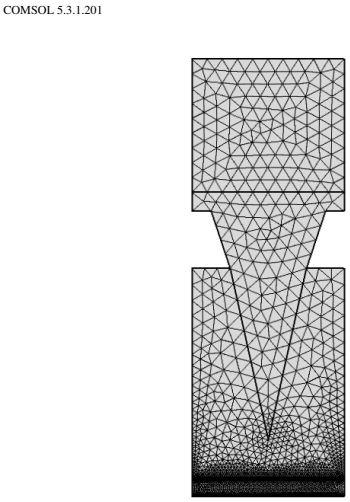

FIGURE 5. Computational mesh.

TABLE 1. Values of the drug diffusivity and water diffusivity in different domains used in the numerical experiments.

sub-domain	free drug diffusivity(m^2/s)	water diffusivity(m^2/s)
Reservoir	1×10^{-11}	3×10^{-10}
Microneedle	7.5×10^{-10}	1.56×10^{-10}
Skin	3.6×10^{-11}	1.56×10^{-10}
Vessel	1×10^{-11}	-

where $\epsilon_1, \epsilon_6 \neq 0$ *satisfy*

$$D_{f,v} - \epsilon_1^2 > 0, \;\; D_{w,m} - \epsilon_6^2 > 0, \tag{3.26}$$

and

$$\Phi = \frac{\min\{2D_{i,j}, 2(D_{f,v} - \epsilon_1^2), 2(D_{w,m} - \epsilon_6^2), \max\{2\iota_{r,m}, 2\iota_{m,s}, 2\iota_{s,v}\}\}}{\max\{\frac{D_v^2\mu}{4\epsilon_6^2 E}, \frac{1}{2\epsilon_1^2}\|\mathbf{v}\|^2_{L^\infty(\Omega_v)}, 2(k_r^2 c_{w,s_0}^2(\epsilon_2^2 + \epsilon_3^2) - k_r c_{w,s_0}), 2(k_m + k_m^2\epsilon_4^2), 2(k_s + k_s^2\epsilon_5^2), \frac{1}{2\epsilon_z^2}, \}}, \tag{3.27}$$

where $i = f, b, w, j = r, m, s, z = 2, 3, 4, 5$.

From the inequality obtained in this theorem, the same results as the previous theorem are obtained.

4. NUMERICAL SOLUTIONS

In this section, the obtained equations are discretized by finite element method using COMSOL Multiphysics 5.3a software. The meshing of different parts is shown in Figure 5. The adaptive differential backward formula with orders between 1 and 2 is used for integration with respect to time. The time step length is considered constant in $0.01s$ after testing the sensitivity of the time step length. The piecewise second-order finite element space is used as P_2 for the concentration and pressure, and the piecewise linear finite element space is used as P_1 for the velocity.

The numerical values of drug and water diffusion coefficient in different domains are represented in Table 1 and other parameters values in Table 2, respectively [29, 31].

To make sure that the numerical results do not depend on the mesh size, we consider the following meshes:

- Mesh 1: 1103 elements;
- Mesh 2: 1469 elements;
- Mesh 3: 4076 elements;

TABLE 2. Values of the other parameters used in the numerical experiments.

Symbol	Explanation	Numerical value
k_r	Solubilisation rate constant($(m^3/(mol.s))$)	6×10^{-9}
$k_j(j = m, s)$	Binding rate constants(1/s)	1×10^{-4}
c_{b,r_0}	Initial bounded drug(mg)	100
c_{w,s_0}	Initial water concentration(mol/m^3)	5.4×10^4
$\iota_{i,j}(i = r, m, s, j = m, s, v)$	Partition coefficients(m/s)	1×10^{-5}
μ_b	The blood viscosity($Pa.s$)	3×10^{-4}
ρ	The blood density(kg/m^3)	5.1×10^5
U	Maximum flow velocity(m/s)	1.2×10^{-7}
D_σ	Viscoelastic diffusion coefficient(Pa)	5×10^{-15}
E	Young modulus(Pa)	10^{-3}
μ	viscosity ($Pa.s$)	10^{-1}

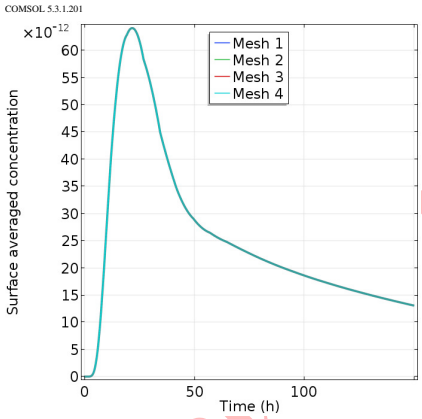

FIGURE 6. Average drug concentration in the blood vessel.

TABLE 3. Different errors for free drug concentration in blood vessel.

h	L^∞	L^2	H^1
0.001	1.3×10^{-12}	1.54×10^{-11}	3.81×10^{-10}
0.01	2.2×10^{-12}	2.14×10^{-11}	5.88×10^{-10}
0.1	3.6×10^{-12}	3.56×10^{-11}	7.43×10^{-10}

- Mesh 4: 11350 elements.

The adequacy of the mesh density has been investigated using convergence tests. Considering two different meshes, the convergence of the solutions and the independence of the mesh have been investigated. To illustrate this claim more clearly, Figure 6 and Table 3 show the comparison among different meshes for the average drug concentration in blood vessel. Of note, the reference solution is defined by $h_{max} = 1 \times 10^{-4}$. According to this figure, the changes among the meshes are almost unrecognizable suggesting that the numerical results do not depend on the mesh size.

We examined the role of drug reservoir in drug delivery through microneedles. Two parameters can play a role in this phenomenon, one being the diffusion coefficient of the drug in the reservoir and the other being the solubility rate of the drug. Once water enters the reservoir, after reacting with the bounded drug, the drug is released and begins to spread. In fact, we examined the effect of these two parameters on the amount of drug reaching the blood vessel.

Figure 7(a) illustrates the effect of diffusion coefficient. In fact, by keeping the solubility rate constant, we change the diffusion coefficient accordingly, by increasing this parameter, the amount of drug reaching the blood vessel rises. Figure 7(b) also demonstrates the effect of solubility rate on drug delivery. In fact, by keeping the diffusion coefficient constant and changing this parameter, we can see that with an increase in the solubility rate, more drug reaches the

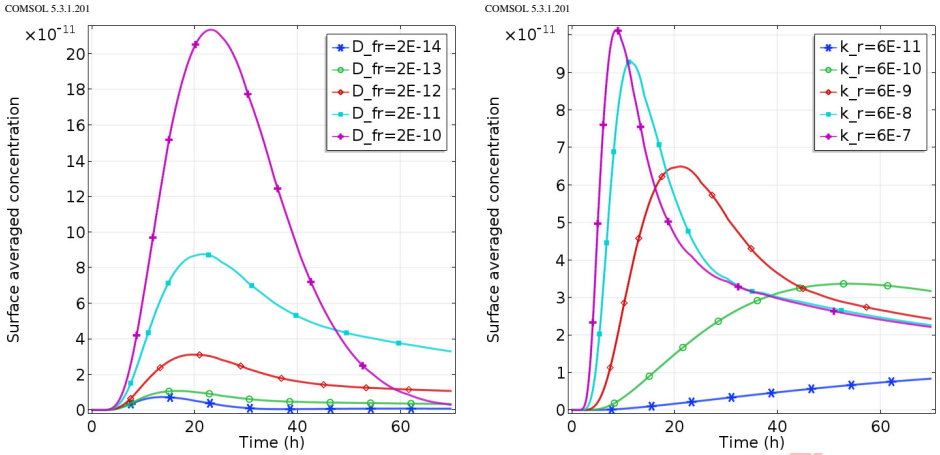

(a) Effect of diffusion coefficient ($D_{f,r}$) (b) Effect of solubility rate (k_r)

FIGURE 7. Average drug concentration in the blood vessel.

blood vessel. The larger the value of this parameter is, the more drug is released, thereby, almost all the bounded drug becomes free drug, and the amount of the released drug reaches its maximum level in less than 10 hours. Compared to the case where we consider the lowest value for this parameter, we saw that less drug is released in the same amount of time and it takes a long time to reach its maximum state. Therefore, drug solubility in the reservoir and its diffusion coefficient in the domain of the reservoir play a major role in drug delivery from the reservoir to the blood vessel through the microneedle. Hence, less solubility of the drug and having a low diffusion coefficient cause less penetration of the drug from the reservoir to the blood vessel.

In order to check the effect of the amount of drug loaded in the reservoir, different amounts of drug, including $80mg$, $90mg$, $100mg$, $110mg$ and $120mg$, are loaded in the reservoir, as shown in Figure 8(a). This figure shows that the time it takes for the drug to reach its maximum state is the same for all the doses, being about 25 hours in all cases. The maximum drug concentration in the blood vessel reaches 8×10^{-5} when $120mg$ drugs are used in the reservoir while it reaches the maximum value of 5×10^{-5} when $80mg$ drugs are loaded in the reservoir.

Another way to evaluate the amount of the drug that has reached the blood vessel is measuring the depth of the microneedle inserted into the reservoir. Cheung indicated that the amount of drug delivered to the blood vessel is directly proportional to the amount of microneedle inserted into the skin [10]. Figure 8(b) exhibits the effect of this phenomenon. In fact, this figure shows the amount of drug concentration in the blood vessel for different depths of microneedle penetration into the skin.

The value of the viscoelastic diffusion coefficient (D_σ), which determines the value of the mechanical property of the polymeric microneedle, ranges between of 3×10^{-15} to 3×10^{-12} to study its effect on drug delivery. As the degree of hardness increases, the flexibility of the polymeric microneedle decreases and the elasticity of the polymer changes, which results in a reduction in the amount of water absorbed by the microneedle. Figure 9(a) shows the change in the amount of water inside the microneedle with different D_σ values. The amount of water increases with a reduction in the value of this parameter. Moreover, the time required for the microneedle to reach the fibers increases. For further clarification, Figure 9(b) illustrates the times between 20 and 40 hours. According to this figure, with the increase in the value of this parameter, the amount of water entering the microneedle declines, indicating that the polymeric microneedle acts as a barrier against the water entering from the skin. Figures 9(c) and 9(d) depict the average concentration of the drug released in the reservoir. With an increase in the value of this parameter, the amount of drug released clearly decreases because with the rise in the value of this parameter, the water entered from the microneedle into the reservoir decreases; less drug is therefore released. Figure 9(d) further explains the time interval between 20 and 40 hours.

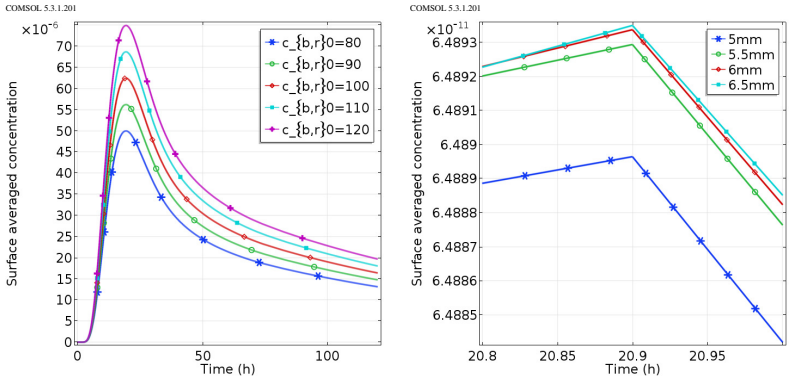

(a) Effect of the amount of drug loaded in the reservoir

(b) Effect of the depth of the microneedle inserted into the reservoir

FIGURE 8. Average drug concentration in the blood vessel.

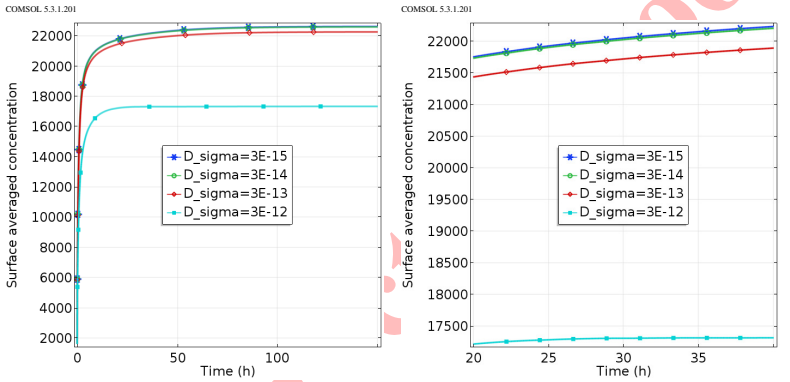

(a) Effect of viscoelastic diffusion coefficient (D_σ).

(b) zoom of (a) for times between 20 and 40 hours

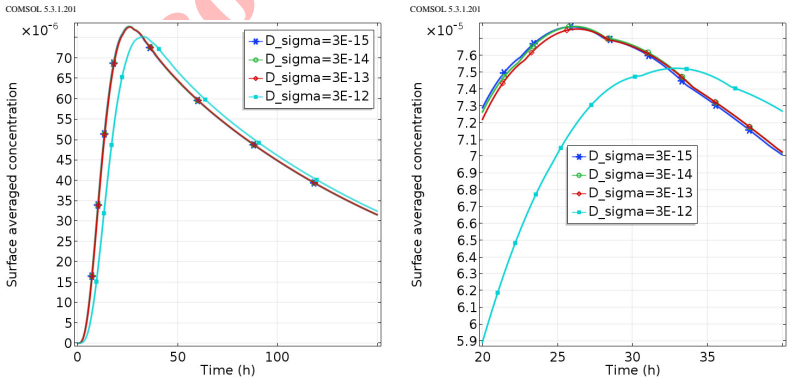

(c) Effect of viscoelastic diffusion coefficient (D_σ)

(d) zoom of (c) for times between 20 and 40 hours

FIGURE 9. Average water concentration in the microneedle ((a) and (b)) and average drug concentration in the reservoir ((c) and (d)).

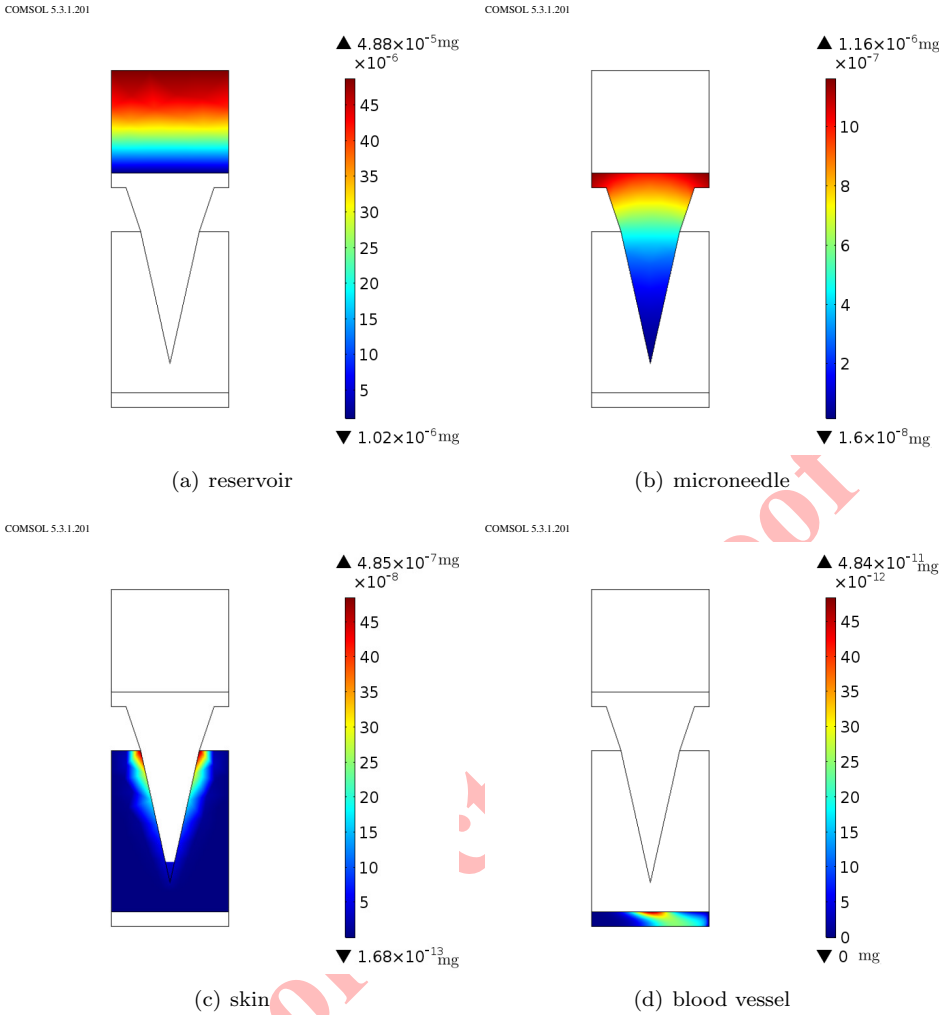

(a) reservoir (b) microneedle

(c) skin (d) blood vessel

FIGURE 10. Free drug concentration ($C_{f,i}, i = r, m, s, v$) in different domains after 150 hours.

Figure 10 shows the concentration of free drug in different domains after 150 hours. The maximum drug concentration value is shown in different figures, which is 4.88×10^{-5} in the reservoir, while being 1.16×10^{-6}, 4.85×10^{-7} and 4.84×10^{-11} in the microneedle, skin and blood vessel, respectively. By comparing these maximum amounts, the amount of drug reaching the blood vessel is almost six times less than that released in the reservoir, which is because of the distance between the reservoir and the blood vessel.

Figure 11(a) shows the comparison of the experimental results with the proposed model for the amount of drug delivered to the bloodstream. The figure clearly shows that the experimental results match what the model predicts. Because some of the loaded drug remains in the reservoir, microneedle, and skin, not all of the drug reaches the bloodstream. Figure 11(b) shows the amount of bound drug in different domains with respect to time. The mass of bound drug in each domain is calculated as the sum of the concentration in each domain. First, the amount of 4 drugs is loaded into the tank, and there is no drug in the microneedle and the skin. Over time, after reacting with water, the bounded drug is released and enters the microneedle. Some of this drug remains in the microneedle due to the reaction between the drug and the polymer. In the same way, some of the drug released from the microneedle enters the skin, and due to drug and tissue reactions, some of this drug remains in the skin.

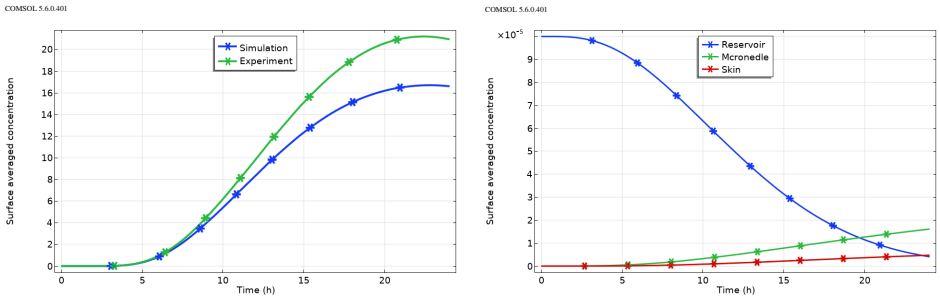

(a) Effect of the amount of drug loaded in the reservoir (b) Effect of the depth of the microneedle inserted into the reservoir

FIGURE 11. Average drug concentration in the blood vessel.

5. Conclusions and future works

A mathematical model was presented by [31] to describe the drug transfer from the reservoir attached to the polymeric microneedle to the blood vessel. Due to the mechanical properties of the polymeric microneedle, which stems from the viscoelastic properties of the polymer, preventing water from entering the skin, the non-Fickian law replaces the Fick's law. The presented model along with the initial and boundary conditions were theoretically and numerically studied and the following results were obtained:

- Studying the stability and uniqueness of the solution of the weak variational formulation by linearizing the model around short and long times (Theorems 3.1 and 3.2);
- The non-dependence of numerical results on the meshing size of the geometry of the problem when using Comsol software (Figure 6 and Table 3);
- The effect of the parameters of diffusion coefficient, $D_{f,r}$, in the reservoir and solubility rate constant, k_r, on the transfer of the drug to the blood vessel (Figure 7);
- Investigating the effect of viscoelastic diffusion coefficient, D_σ, on the water entering from the skin into the polymeric microneedle (Figure 9).
- The results are in good agreement with the numerical and experimental results (Figure 11(a)).

In this paper, the viscoelastic property of microneedles was investigated when water enters the microneedle from the skin, and the polymer acts as a barrier. The same barrier exists when the water exits the microneedle and enters the reservoir, when the free drug enters the microneedle, and when the free drug exits the microneedle and enters the skin. For the sake of simplicity, this feature was investigated only once water entered the microneedle from the skin, and a similar result was obtained.

The swelling of the microneedle after water enters the skin causes a time-dependent change in the boundary between the microneedle and the skin. As a result, the domain of the mathematical solution of the transfer equations also changes with time, leading to the moving boundary problem. In near future, we will delve into this problem and investigate it.

Statements and Declarations

Competing interests There is no Competing interests.

Data Availability

All data generated or analysed during this study are included in this published article.

Acknowledgments

The authors would like to express their profound gratitude to the editor and anonymous reviewers for their remarkable dedication and invaluable feedback, which greatly enhanced the quality of the paper.

References

[1] B. Ahn, *Optimal Microneedle Design for Drug Delivery Based on Insertion Force Experiments with Variable Geometry*, Int. J. Control Autom. Syst., (2019), 1–7.
[2] E. Azhdari, J. A. Ferreira, P. De Oliveira, and P. M.Da Silva, *Diffusion, viscoelasticity and erosion: analytical study and medical applications*, J Comput Appl Math, *275* (2015), 489–501.
[3] E. Azhdari, J. A. Ferreira, P. de Oliveiraa, and P. M. da Silva *Numerical and analytical study of drug release from a biodegradable viscoelastic platform*, Mathematical Methods in the Applied Sciences, *39*(16) (2015), 4688-4699.
[4] E. Azhdari, and J. Naghipoor, *The effect of viscoelasticity of the tissue on the magneto-responsive drug delivery system*, J. Math. Biol., *84*(13) (2022), 1–26.
[5] S. Bhatnagar, P. R. Gadeela, P. Thathireddy, and V. V. K. Venuganti, *Microneedlebased drug delivery: materials of construction*, J. Chem. Sci., *131* (2019), 90.
[6] M. Bok, Z. Zhao, S. Jeon, J. Jeong, and E. Lim, *Ultrasonically and iontophoretically enhanced drug-delivery system based on dissolving microneedle patches*, Scientific Rep., *10*(1) (2020), 1–10.
[7] H. F. Brinson, and L. C. Brinson, *Polymer engineering science and viscoelasticity: an introduction*, Springer, New York, 2010.
[8] A. Carcamo-Martinez, B. Mallon, J. Dominguez-Robles, L. K. Vora, Q. K. Anjani, and R. F. Donnelly, *Hollow microneedles: A perspective in biomedical applications*, Int. J. Pharm., *599* (2021).
[9] K. Cheung, and D. Das, *Microneedles for drug delivery: trends and progress*, 2014.
[10] K. Cheung, T. Han, and D. B. Das, *Effect of Force of Microneedle Insertion on the Permeability of Insulin in Skin*, J. Diabetes Sci. Technol, *8*(3) (2014), 444–452.
[11] A. Davidson, B. Al-Qallaf, and D. B. Das, *Transdermal drug delivery by coated microneedles: Geometry effects on effective skin thickness and drug permeability*, Chem. Eng. Res. Des., *86* (2008), 1196–1206.
[12] S. Dharadhar, A. Majumdar, S. Dhoble, and V. Patravale, *Microneedles for transdermal drug delivery: a systematic review*, Drug Dev Ind Pharm., *45*(2) (2019), 188–201.
[13] R. F. Donnelly, K. Mooney, E. Caffarel-Salvador, B. M. Torrisi, E. Eltayib, and J. C. McElnay, *Microneedle-mediated minimally invasive patient monitoring*, Ther. Drug Monit., *36*(1) (2014), 10–17.
[14] S. Duarah, M. Sharma, and J. Wen, *Recent advances in microneedle-based drug delivery: Special emphasis on its use in paediatric population*, Eur. J. Pharm. Biopharm., *136* (2019), 48–69.
[15] L. Evans, *Partial Differential Equations*, American Mathematical Society, Providence, Rhode Island, Second Edition, 2010.
[16] J. Ferreira, M. Grassi, E. Gudino, and P. de Oliveira, *A new look to nonfickian diffusion*, Applied Mathematical Modelling, *39*(1) (2014), 194–204.
[17] J. A. Ferreira, M. Grassi, E. Gudino, and P. de Oliveira, *A 3D model for mechanistic control drug release*, SIAM Journal on Applied Mathematics, *74* (2014), 620-633.
[18] M. Guzmán-Alonso, and T. Cortázar, *Water content at different skin depths and the influence of moisturizing formulations*, 2016.
[19] S. Henry, D. V. McAllister, M. G. Allen, and M. R. Prausnitz, *Micromachined needles for the transdermal delivery of drugs*, Proc. MEMS 98. IEEE. Elev. Annu. Int. Work. Micro Electro Mech. Syst. An Investig. Micro Struct. Sensors, Actuators, Mach. Syst. (Cat. No. 98CH36176).
[20] K. S. Kim, K. Ita, and L. Simon, *Modelling of dissolving microneedles for transdermal drug delivery: Theoretical and experimental aspects*, Eur. J. Pharm. Sci., *68* (2015), 137–143.
[21] E. Larraneta, and L. Vora, *Microneedles for Drug and Vaccine Delivery and Patient Monitoring*, John Wiley and Sons, Ltd, Chichester, UK, (2018), 177–205.
[22] M. Li, L. K. Vora, K. Peng, and R. F. Donnelly, *Trilayer microneedle array assisted transdermal and intradermal delivery of dexamethasone*, Int. J. Pharm., (2021).

[23] G. Pontrelli, and F. de Monte, *A two-phase two-layer model for transdermal drug delivery and percutaneous absorption*, Math. Biosci, *257* (2014), 96–103.
[24] S. Puttipipatkhachorn, J. Nunthanid, K. Yamamoto, and G. E. Peck, *Drug physical state and drug-polymer interaction on drug release from chitosan matrix films*, J. Control. Release, *75*(1-2) (2001), 143–153.
[25] S. Rojekar, L. K. Vora, I. A. Tekko, F. Volpe-Zanutto, H. O. McCarthy, P. R. Vavia, and R. F. Donnelly, *Etravirine-loaded dissolving microneedle arrays for longacting delivery*, Eur. J. Pharmaceut. Biopharmaceut., *165* (2021), 41–51.
[26] P. Ronnander, L. Simon, and A. Koch, *Experimental and mathematical study of the transdermal delivery of sumatriptan succinate from polyvinylpyrrolidonebased microneedles*, Eur. J. Pharm. Biopharm., *146* (2020), 32–40.
[27] S. P. Timoshenko, and J. M. Gere, *Theory of elastic stability*, Courier Corporation, 2009.
[28] C. Uppuluri, A. S. Shaik, T. Han, A. Nayak, K. J. Nair, B. R. Whiteside, B. N. Nalluri, and D. B. Das, *Effect of microneedle type on transdermal permeation of rizatriptan*, Aaps Pharmscitech, *18* (2017), 1495–1506.
[29] P. R. Yadav, L. J. Dobson, S. K. Pattanayek, and D. B. Das, *Swellable Microneedles Based Transdermal Drug Delivery: Mathematical Model Development and Numerical Experiments*, Chemical Engineering Science, *247* (2022).
[30] P. R. Yadav, M. N. Munni, L. Campbell, G. Mostofa, L. Dobson, M. Shittu, S. K. Pattanayek, M. Uddin, and D. B. Das, *Translation of Polymeric Microneedles for Treatment of Human Diseases: Recent Trends, Progress, and Challenges*, Pharmaceutics, *13*(8) (2021), 1132.
[31] P. R. Yadav, M. I. Nasiri, L. K. Vora, E. Larraneta, R. F. Donnelly, S. K. Pattanayek, and D. B. Das, *Super-swelling hydrogel-forming microneedle based transdermal drug delivery: Mathematical modelling, simulation and experimental validation*, International Journal of Pharmaceutics, *622* (2022), 1–14.
[32] P. R. Yadav, and S. K. Pattanayek, *Modulation of Physicochemical Properties of Polymers for Effective Insulin Delivery Systems BT - Biointerface Engineering: Prospects in Medical Diagnostics and Drug Delivery*, In: Chandra, P., Pandey, L. M. (Eds.), Springer Singapore, Singapore, (2020), 123–148.